

# Universal Amplitude Equation at the Onset of Pattern Formation for General Non-local and Non-linear Models

Stefano Garlaschi,<sup>\*</sup> Deepak Gupta,<sup>\*</sup> Amos Maritan,<sup>†</sup> and Sandro Azaele<sup>†</sup>

*Dipartimento di Fisica e Astronomia Galileo Galilei,  
Università degli studi di Padova, via Marzolo 8, 35131 Padova, Italy*

(Dated: March 3, 2022)

The remarkable empirical finding that extensive fine-scale diversity is stable on long time scales, despite selective pressures, has spurred the study of several models, which can explain species formation and stability. However, the focus has been more on the possible mechanisms which sustain coexistence, rather than on their universality and robustness. We thus consider a model that includes generic forms of many-body non-linear interactions, which are non-local and depend on a set of parameters. Despite the complicated dynamics, we are able to aptly identify a region in the parameter space where the dynamics manifests universal and robust features which extend to the weakly non-linear regime. Large scale variations of patterns are well captured by a Ginzburg-Landau equation, whose form does not depend on the details of the underlying models. The mathematical framework we have introduced has much larger applicability than the one considered here, possibly including pattern formation in models with very different physical features. The analytical predictions yield a good agreement when compared to the numerical integration of a competitive Lotka-Volterra equation with non-local interactions.

One of the basic mechanisms underpinning the formation of spatial structures is the instability of spatially uniform, and stationary, states under small perturbations. This simple mechanism is the beginning of pattern formation [1–3] and has yielded valuable insights into natural and controlled non-equilibrium systems. The diversity of spatial patterns can be investigated by means of this approach in a wealth of systems, ranging from the archetypal Rayleigh-Bénard convection [4–7] to reaction-diffusion systems [8–12]. These latter include reactions of chemical species, eventually leading to regular patterns in coats and skins of animals [13, 14] or seashells [15].

In the evolution equation an essential role is played by the non-linear terms that are able to stabilise the initial growth of perturbations and eventually select the spatial pattern. In many examples of interest, including those we have alluded to above, non-linearities are assumed to be local, albeit spatial patterns can be generated by more general forms of nonlinear terms.

For instance, the Phase Field Crystal (PFC) theory incorporates crystalline details on length and time scales of experimental relevance and is used to model the structure of several materials [16, 17]. The connection to the microscopic details is achieved via the Dynamic Density Functional (DDF) theory, from which it can be derived [18]. In the DDF theory the pairwise and higher order spatial correlation functions are responsible for the non-local (and non-linear) contributions, which govern the evolution of the conserved order parameter.

Non-local models have also played an important role in theoretical ecology. They have been used to explain regular alternation of colonized and uncolonized regions in vegetation landscapes [19, 20] and how species may originate [21]. Competition can indeed lead to formation of species by limiting their similarity and partitioning

environmental resources [22]. The intertwining combination of competition and environmental effects is usually modelled by assuming that species undergo a diffusion process and non-local interactions in the space of their traits. The eventual patterns are a hallmark of the surviving species [23, 24].

Linear stability analysis provides the first and easiest insight into pattern formation. We gain understanding of the modes which drive instability, and therefore determine length and time scales characteristic of the spatial structures. Typically, these structures are distorted over either large length or large temporal scales, and these slow changes cannot be determined by a simple linear analysis. However, near the onset of instability, in the weakly non-linear regime, it is possible to deduce the evolution equation of the amplitude of the most unstable modes, which captures the basic information about those distortions and their relative scales. Naïvely, one could expect that non-linearity along with non-locality may give rise to a phenomenology of patterns with no universal features. However, in this Letter we show that, under fairly general assumptions, the amplitude equation does not depend on the details of the specific model. The envelope of such patterns is governed by a universal equation near the onset of instability. This occurs quite generally for both local and non-local interactions and in presence of  $n$ -body interactions,  $n \geq 2$ , such as in a non-local competitive Lotka-Volterra equation and also when investigating dynamics generalizing the celebrated *Swift-Hohenberg* model [5, 25, 26].

Here we investigate pattern formation in systems whose evolution is characterized by a general non-local non-linear dynamics. For the sake of simplicity we study the dynamics of a real field  $\phi(x, t)$ , which is governed by the following equation in one spatial dimension (the

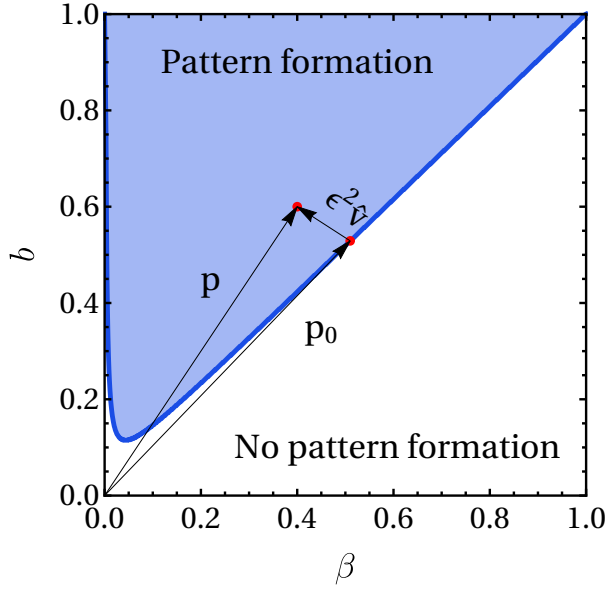


FIG. 1. Phase diagram in the  $(\beta, b)$  space for the non-local CLV model given in Eqs. (1) and (4) with  $F_{\mathbf{q}}[u, v] := u[1 - av]$ . In this case  $\mathbf{p} \equiv \{\beta, b, R, a, D\}$  and the critical hyper-surface  $\mathcal{M}$  does not depend on  $a$ . The phase diagram is shown for two fixed parameters  $D = 10^{-8}$  and  $R = 0.1$ , where the solid contour  $\mathcal{M}$  [defined by  $\lambda_{\mathbf{p}_0}(k_M(\mathbf{p}_0)) = 0$ ] divides the parameter space depending on whether or not there is pattern formation. A vector  $\mathbf{p} = \mathbf{p}_0 + \epsilon^2 \hat{v}$  indicates a point in the pattern forming region, where  $\mathbf{p}_0$  sits on  $\mathcal{M}$ .

generalization to higher dimensions is straightforward)

$$\partial_t \phi(x, t) = F_{\mathbf{q}}[\phi(x, t), (G_{\mathbf{q}} * \phi)(x, t)] + D \partial_x^2 \phi(x, t), \quad (1)$$

where  $F_{\mathbf{q}}(\cdot, \cdot)$  is an analytic function,  $\mathbf{q}$  indicates a set of parameters and  $D$  a diffusion constant. The non-local contribution to the equation comes from the convolution, i.e.,  $(G_{\mathbf{q}} * \phi)(x, t) := \int_{-\infty}^{+\infty} G_{\mathbf{q}}(x - y) \phi(y, t) dy$ , of the field with the smooth even function  $G_{\mathbf{q}}(\cdot)$ . Note that in our formulation, we are not considering the contribution from the spatial boundaries. Therefore, we can perform the integral over the  $x$ -variable from  $-\infty$  to  $+\infty$ . The inclusion of other non-local contributions with higher-order interactions such as

$$\int G_{\mathbf{q}}(x - y_1, x - y_2, \dots, x - y_n) \prod_{i=1}^n [\phi(y_i, t) dy_i] \quad (2)$$

in the function  $F_{\mathbf{q}}$  in Eq. (1) is also straightforward to handle and does not change the main result (9). We emphasize that Eq. (1) generalizes several models, including the competitive Lotka-Volterra (CLV) equation [23, 27, 28] and some reaction-diffusion models [9, 29].

We indicate with  $\phi_{\mathbf{q}}^{(0)}$  the homogeneous and stationary solution of Eq. (1), i.e.,  $F_{\mathbf{q}}[\phi_{\mathbf{q}}^{(0)}, \tilde{G}_{\mathbf{q}}(k = 0) \phi_{\mathbf{q}}^{(0)}] = 0$ , where  $\tilde{G}_{\mathbf{q}}(k) = \int_{-\infty}^{+\infty} dz G_{\mathbf{q}}(z) e^{ikz}$  is the Fourier transform of  $G_{\mathbf{q}}$ . Spatial patterns that form in the weakly

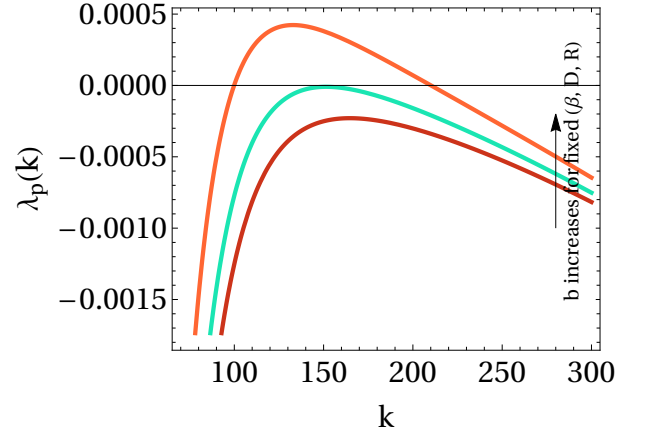


FIG. 2. The plot shows  $\lambda_{\mathbf{p}}(k)$ , the dispersion relation given in Eq. 6, as a function of  $k$  for the non-local CLV model at three different values of  $b$ . The remaining parameters are  $\beta = 0.2$ ,  $D = 10^{-8}$ , and  $R = 0.1$ .

non-linear regime can be investigated in the region of instability around  $\phi_{\mathbf{q}}^{(0)}$ . Therefore, we substitute  $\phi_k(x, t) = \phi_{\mathbf{q}}^{(0)} + \delta e^{\lambda_{\mathbf{p}}(k)t + ikx} + c.c.$  into Eq. (1), assuming that the spatially harmonic perturbation is uniformly small, namely  $0 < \delta \ll 1$ . Up to first order in  $\delta$ , the growth rate  $\lambda_{\mathbf{p}}(k)$  as a function of wave number  $k$  reads

$$\lambda_{\mathbf{p}}(k) = (1, \tilde{G}_{\mathbf{q}}(k)) \cdot \nabla F_{\mathbf{q}}|_{(\phi_{\mathbf{q}}^{(0)}, \tilde{G}_{\mathbf{q}}(0) \phi_{\mathbf{q}}^{(0)})} - D k^2, \quad (3)$$

where  $\mathbf{p} \equiv \{\mathbf{q}, D\}$  refers to the set of all parameters of the model and  $\nabla F_{\mathbf{q}}|_{(x^*, y^*)} = [\partial_x F_{\mathbf{q}}(x, y)|_{(x^*, y^*)}, \partial_y F_{\mathbf{q}}(x, y)|_{(x^*, y^*)}]^T$ . Because we assume that  $G_{\mathbf{q}}(x)$  is even, the quantity  $\lambda_{\mathbf{p}}(k)$  is a real function. The mode  $k$  is unstable if the corresponding growth rate  $\lambda_{\mathbf{p}}(k)$  is positive. Let  $k_M(\mathbf{p})$  be the wave number corresponding to the absolute maximum of the growth rate. It satisfies  $\partial_k \lambda_{\mathbf{p}}(k)|_{k=k_M(\mathbf{p})} = 0$  and for brevity we set  $\lambda_M \equiv \lambda_{\mathbf{p}}(k_M(\mathbf{p}))$ . Thus, the *critical hyper-surface* is the set of points where  $\lambda_M$  is zero, i.e., the set of points  $\mathbf{p}_0 \equiv \{\mathbf{q}_0, D_0\}$  satisfying the equation  $\lambda_{\mathbf{p}_0}(k_M(\mathbf{p}_0)) = 0$ . Such hyper-surface, which we call  $\mathcal{M}$ , separates the parameter space into two regions, depending on the stability of  $\phi_{\mathbf{q}}^{(0)}$  (see Fig. 1).

As an exemplification of our formalism we will keep in mind the case corresponding to a non-local CLV equation with two-body interactions. In this model a species is represented by a point in the niche space. Species interact with each other according to the kernel

$$G_{\mathbf{q}}(z) = e^{-\frac{|z|}{R}} - b e^{-\frac{|z|}{\beta R}}, \quad (4)$$

which we have chosen because it is amenable to analytical calculations.  $R$  is the range of the interaction,  $\beta$  and  $b$  are dimensionless parameters and  $0 < b, \beta < 1$ . In this example the first term on the right-hand side of Eq. (1)

has the form

$$F_{\mathbf{q}}[u, v] := u[1 - av], \quad (5)$$

where  $a$  is the inverse of a carrying capacity in this example. Herein, the homogeneous and stationary solution is  $\phi_{\mathbf{q}}^{(0)} = [a\tilde{G}_{\mathbf{q}}(0)]^{-1}$ . From Eq. (3), the dispersion relation can be expressed as

$$\lambda_{\mathbf{p}}(k) = \frac{1}{1 - b\beta} \left( \frac{b\beta}{\beta^2 k^2 R^2 + 1} - \frac{1}{k^2 R^2 + 1} \right) - D k^2 \quad (6)$$

where  $\mathbf{p} = \{b, \beta, a, R, D\}$  is the set of parameters and  $\lambda_{\mathbf{p}}(k)$  does not depend on  $a$ . We plot  $\lambda_{\mathbf{p}}(k)$  in Fig. 2 for three different values of  $b$ , while the other parameters are fixed. The phase diagram corresponding to  $\lambda_{\mathbf{p}}(k)$  given in Eq. (6) is shown in Fig. 1, where the blue shaded region points out the region of pattern formation.

In order to make analytical progress we use the Taylor series expansion of the right-hand side of Eq. (1) around the homogeneous and stationary solution  $\phi_{\mathbf{q}}^{(0)}$ . This allows to set up the equations that hold in the weakly non-linear regime and finally obtain the amplitude equation. We express the field as  $\phi(x, t) = \phi_{\mathbf{q}}^{(0)} + \varphi(x, t)$ , and consider  $\varphi(x, t)$  to be small compared to  $\phi_{\mathbf{q}}^{(0)}$ . The evolution equation for  $\varphi(x, t)$  can then be cast in the form

$$\partial_t \varphi(x, t) = \mathcal{L}_{\mathbf{p}} \varphi + \sum_{\substack{n, m=0 \\ n+m \geq 2}}^{+\infty} C_{\mathbf{q}}^{(n, m)} \varphi^n (G_{\mathbf{q}} * \varphi)^m, \quad (7)$$

where  $C_{\mathbf{q}}^{(n, m)}$  are the coefficients of the Taylor expansion and  $\mathcal{L}_{\mathbf{p}}$  is the linear and non-local operator, defined as  $\mathcal{L}_{\mathbf{p}} \varphi = (\varphi, G_{\mathbf{q}} * \varphi) \cdot \nabla F_{\mathbf{q}}|_{\phi_{\mathbf{q}}^{(0)}, \tilde{G}_{\mathbf{q}}(0)\phi_{\mathbf{q}}^{(0)}} + D \partial_x^2 \varphi$ , which will play an important role in the following. For example, in the CLV model the linear operator acting on the perturbation field  $\varphi$  has the form  $\mathcal{L}_{\mathbf{p}} \varphi = -[\tilde{G}_{\mathbf{q}}(0)]^{-1} (G_{\mathbf{q}} * \varphi) + D \partial_x^2 \varphi$ , and the second term on the right-hand side of Eq. (7) is  $-a \varphi (G_{\mathbf{q}} * \varphi)$ . Since Eq. (1) is translational invariant, the eigenfunctions of the linear non-local operator  $\mathcal{L}_{\mathbf{p}}$  are the simple wavefunctions  $e^{ikx}$ . Thus, the eigenvalue equation reads  $\mathcal{L}_{\mathbf{p}} e^{ikx} = \lambda_{\mathbf{p}}(k) e^{ikx}$ , where the spectrum is defined in Eq. (3). The general solution of the linear part of Eq. (7), i.e.,  $\partial_t \varphi(x, t) = \mathcal{L}_{\mathbf{p}} \varphi$ , is a linear combinations of functions  $e^{\lambda_{\mathbf{p}}(k)t + ikx}$  with  $k$  dependent coefficients.

We now investigate the behavior of the system close to the onset of instability, namely near the critical hyper-surface  $\mathcal{M}$ . Thus, we consider parameters  $\mathbf{p}$  in the neighborhood of  $\mathbf{p}_0 \equiv \{\mathbf{q}_0, D_0\}$ , i.e.,  $\mathbf{p} = \mathbf{p}_0 + \epsilon^2 \hat{v}$ , where  $\mathbf{p}_0 \in \mathcal{M}$ ,  $\hat{v}$  is a unit vector pointing toward the region of pattern formation, and  $0 < \epsilon^2 \ll 1$ . An example of such point  $\mathbf{p}$  is indicated in Fig. 1. With this assumption, we expand the right-hand side of Eq. (7) around  $\mathbf{p}_0$  in powers of  $\epsilon$ . In addition, we assume that the growth rate  $\lambda_{\mathbf{p}}(k)$  exhibits a quadratic scaling in the wave-number  $k$

close to the point of maximum  $k_M(\mathbf{p}) > 0$ , which is satisfied if  $\lambda_{\mathbf{p}}(k)$  admits continuous second derivative with respect to  $k$  [30].

We find that the maximum scales like  $\epsilon^2$  as  $\epsilon \rightarrow 0^+$  [30], i.e.,  $\lambda_M \equiv \lambda_{\mathbf{p}}(k_M(\mathbf{p})) \sim \epsilon^2 \bar{\lambda}_M$  as  $\epsilon \rightarrow 0^+$ , where we introduce the re-scaled quantity  $\bar{\lambda}_M$ , which is  $\mathcal{O}(1)$ . Owing to this scaling property, we can introduce a temporal- and spatial-scale separation which simplifies Eq. (7). The long time deviations from the fast oscillations evolve on scales determined by the slower time variable  $\tau = \epsilon^2 t$ . A similar spatial-scale separation for the perturbation field  $\varphi(x, t)$  occurs with a spatial scale given by the slower variable  $\xi = \epsilon x$ . Therefore, we write  $\varphi(x, \xi, \tau)$  as a power series in  $\epsilon$ , i.e.,  $\varphi(x, \xi, \tau) = \sum_{j \geq 1} \epsilon^j \varphi_j(x, \xi, \tau)$ , where the time dependence in each mode on the right-hand side is through  $\tau$ . Similarly the spatial dependence appears both through the  $x$  and the slower variable  $\xi$  [2].

Using these considerations and comparing like terms in  $\epsilon$  in Eq. (7), we find that  $\varphi_1(x, \xi, \tau)$  is harmonic and its mode is determined by the critical wave-number at  $\mathbf{p}_0$ ,  $k_M(\mathbf{p}_0)$  (see [30] for detailed calculations),

$$\varphi_1(x, \xi, \tau) = A(\xi, \tau) e^{ik_M(\mathbf{p}_0)x} + \bar{A}(\xi, \tau) e^{-ik_M(\mathbf{p}_0)x}, \quad (8)$$

where  $A(\xi, \tau)$  is the amplitude of the harmonic perturbation, and  $\bar{A}(\xi, \tau)$  is its complex conjugate. Thus, near the critical hyper-surface the emergent key variable is represented by the amplitude of the pattern  $A(\xi, \tau)$ , which depends only on slow variables.

The growth equation for  $A(\xi, \tau)$  can be found ensuring that the higher-order terms in the expansion of Eq. (7) are well defined [30]. We eventually find

$$\frac{\partial A}{\partial \tau} = \bar{\lambda}_M A - \alpha |A|^2 A + \frac{1}{2} |\lambda_{\mathbf{p}_0}''(k_M(\mathbf{p}_0))| \frac{\partial^2 A}{\partial \xi^2}, \quad (9)$$

where we have dropped the dependence  $\xi$  and  $\tau$  from  $A(\xi, \tau)$ . In the above equation all coefficients on the right-hand side depend on  $\mathbf{p}_0$ , and the detailed expression of the constant  $\alpha$  in terms of model details is given in [30].

Eq. (9) represents our main result. Our derivation show that this equation is universal, i.e., the only model dependence enters through the three coefficients appearing on the right-hand side of Eq. (9), which depend on the specificity of Eq. (1). Eq. (9) emerges very generally, of which Eq. (1) is a prototype, at the onset of the instability between a region with uniform steady state and a region with patterns that lead to the breaking of translational invariance.

Interestingly, Eq. (9) is the celebrated Ginzburg-Landau (GL) equation for a complex field  $A(\xi, \tau)$ , which was first obtained for the Swift-Hohenberg model. Our general approach shows that the behaviour predicted by the GL equation describes the phenomenology emerging from a much larger class of models and it is not only limited to generalizations of the Swift-Hohenberg model [25, 26].

We confirm the predictions of Eq. (9) with the numerical integration of the CLV model. For fixed parameters  $\mathbf{p}$  and  $\mathbf{p}_0$ , we consider two simple cases, which differ by the choice of the initial conditions used in the amplitude equation as well as for the evolution of the CLV model.

In the first case, we consider an initial real homogeneous amplitude  $A(\xi, 0) = A_0 \in \mathbb{R}$ , used to set the corresponding initial condition adopted in the CLV dynamics [30]. Owing to this choice, the amplitude remains space-independent at any time, displaying only temporal changes. In Fig. 3, we show that the comparison between an analytical prediction of Eq. (9) and the numerical integration of Eq. (1), using Eqs. (4) and (5), is quite accurate at all times. In the second case, aiming to study a spatial-dependent scenario for the amplitude, we use as initial condition a particular stationary solution of Eq. (9) (discussed in [30]). The carrier wave obtained from the numerical integration up to  $10^2$  time steps shows a remarkable agreement with the analytical solution calculated in the weakly non-linear regime. For the sake of clarity, Fig. 4 illustrates the envelope of the carrier wave highlighted with red colour. This is the curve  $\phi_{\mathbf{q}}^{(0)} + 2\epsilon A_{st}(\xi)$ , where  $A_{st}(\xi)$  is a stationary solution of Eq. (9). This agreement confirms the validity of our findings also for spatially modulated patterns. The numerical amplitude showed in Fig. 3 and the predicted envelope displayed in Fig 4 are obtained by taking into account only the first order term (8) of the perturbative expansion. In [30] we present the results for the numerical evaluation of the amplitude when considering the next-to-leading order terms.

In this paper, starting from a general model defined in the niche space, we have showed that species emerge as a trade-off between non-local interactions and their tendency to scour the space for better evolutionary solutions. We find regularly spaced lumps of species, showing a general tendency of species to coexist when they are either sufficiently similar or sufficiently different, with typical distance of lumps  $\mathcal{O}(k_M^{-1}(\mathbf{p}_0))$  along a niche axis. Such patterns do not form because of the specificity of the model, but as a consequence of the universality which operates near the instability. Universality and robustness of our findings extend to the large scale modulation of patterns as described by the GL equation, Eq. (9). This is particularly interesting for the implications. The key steps in our derivations – e.g., the introduction of the non-local linear operator  $\mathcal{L}_{\mathbf{p}}$ , the expansion close to the boundaries of the critical hyper-surface  $\mathcal{M}$  where a quadratic scaling occurs – could equally well be applied to models with different physical features. For instance, non-local higher-order interactions may play an important role in shaping patterns of ecological communities and may also help to stabilize their dynamics [31]. Close to instability, those terms will affect only the coefficients of the GL equation. Also, by replacing  $F_{\mathbf{q}}$  with  $\partial_x^2(\delta\mathcal{F}_{\mathbf{q}}/\delta\phi)$  in Eq.(1),

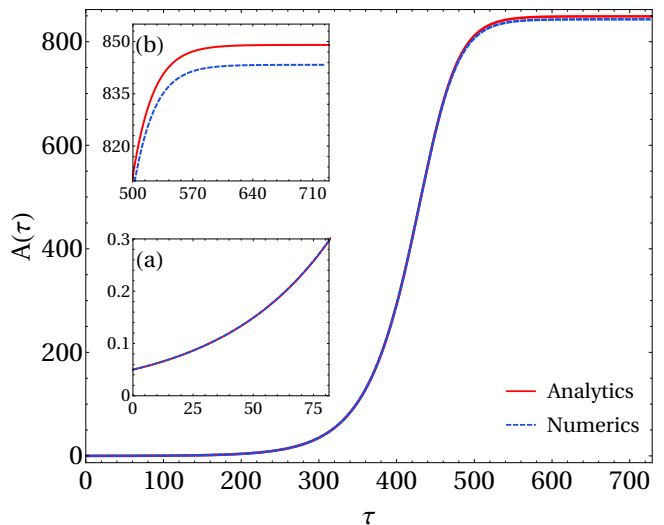


FIG. 3. Comparison between the growth in time of the amplitude predicted by Eq. (9) from the initial condition  $A(\xi, \tau = 0) = A_0 = 0.05$  (solid red line) and the corresponding numerical evaluation (blue dashed line) from the integration of the CLV model using  $\phi(x, \xi, 0) = \phi_{\mathbf{q}}^{(0)} + 2\epsilon A_0 \cos(k_M(\mathbf{p}_0)x)$  as an initial condition [30]. We refer to [30] for the details of the parameters  $\mathbf{p}$  and  $\mathbf{p}_0$  used in both analytics and numerical simulation. The insets show the zoom on the initial growth (a) and the saturation observed at large time (b).

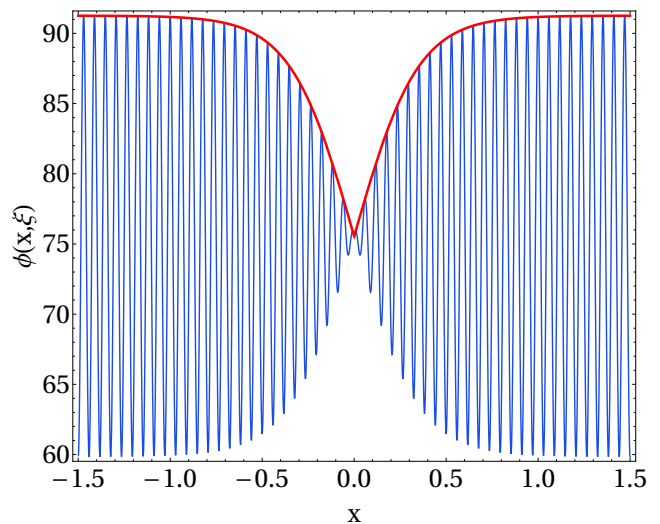


FIG. 4. Comparison between the spatially-dependent stationary solution of Eq. (9),  $A_{st}(\xi)$ , presented in [30] (the red solid line is the envelope curve  $\phi_{\mathbf{q}}^{(0)} + 2\epsilon A_{st}(\xi)$ , where  $\xi = \epsilon x$ ) and the solution obtained from the numerical intergration of the CLV dynamics using  $\phi(x, \xi, 0) = \phi_{\mathbf{q}}^{(0)} + 2\epsilon A_{st}(\xi) \cos(k_M(\mathbf{p}_0)x)$  as initial condition. This plot is obtained at time  $t = 10^2$  (time steps). The parameters  $\mathbf{p}$  and  $\mathbf{p}_0$  along with a discussion of this solution are included in [30].

we could describe the dynamics of a conserved order parameter as we have alluded to in the introduction. Large scale modulation of patterns of such fields may still be described by GL equations. Finally, generalized GL equations for many amplitudes could be derived for systems with many interacting species' populations (or different order parameters)  $\phi_m(x, t)$ , where the discrete index  $m$  represents the trophic level to which they belong.

S. G. acknowledges the support from Univeristy of Padova through the PhD fellowship within Bando Dottorati di Ricerca, funded by Fondazione Cassa di Risparmio di Padova e Rovigo. D. G. and A. M. acknowledge the support from University of Padova through Excellence Project 2018 of Fondazione Cassa di Risparmio di Padova e Rovigo. We thank Samir Suweis for useful discussions.

---

\* Equal junior contribution

† Equal senior contribution

- [1] Cross, M. and Greenside, H., 2009. Pattern formation and dynamics in nonequilibrium systems. Cambridge University Press.
- [2] Hoyle, R. and Hoyle, R.B., 2006. Pattern formation: an introduction to methods. Cambridge University Press.
- [3] Murray, J.D., 2001. Mathematical biology II: spatial models and biomedical applications. New York: Springer.
- [4] Subrahmanyan Chandrasekhar. Hydrodynamic and hydromagnetic stability. Courier Corporation, 2013.
- [5] Mark C Cross and Pierre C Hohenberg. Pattern formation outside of equilibrium. *Reviews of modern physics*, 65(3):851, 1993.
- [6] Jean Karl Platten and Jean Claude Legros. Convection in liquids. Springer Science & Business Media, 2012.
- [7] RC Di Prima and Harry L Swinney. Instabilities and transition in flow between concentric rotating cylinders. *Hydrodynamic instabilities and the transition to turbulence*, pages 139–180. Springer, 1981.
- [8] Nabika, H., Itatani, M. and Lagzi, I., 2019. Pattern Formation in Precipitation Reactions: the Liesegang Phenomenon. *Langmuir*.
- [9] Alan Mathison Turing. The chemical basis of morphogenesis. *Bulletin of mathematical biology*, 52(1-2):153–197, 1990.
- [10] Bánsági, Tamás and Vanag, Vladimir K and Epstein, Irving R. Tomography of reaction-diffusion microemulsions reveals three-dimensional Turing patterns. *Science*, 331(6022):1309–1312, 2011.
- [11] Castets, Vincent and Dulos, Etienne and Boissonade, Jacques and De Kepper, Patrick. Experimental evidence of a sustained standing Turing-type nonequilibrium chemical pattern. *Physical review letters*, 64(24):2953, 1990.
- [12] Ouyang, Qi and Swinney, Harry L. Transition from a uniform state to hexagonal and striped Turing patterns. *Nature*, 352(6336):610–612, 1991.
- [13] James D Murray. *Mathematical biology*, volume I, an introduction, 2002.
- [14] Nakamasu, Akiko and Takahashi, Go and Kanbe, Akio and Kondo, Shigeru. Interactions between zebrafish pigment cells responsible for the generation of Turing patterns. *Proceedings of the National Academy of Sciences*, 106(21):8429–8434, 2009.
- [15] Meinhardt, H. and Klingler, M., 1987. A model for pattern formation on the shells of molluscs. *Journal of Theoretical Biology*, 126(1), pp.63–89.
- [16] Boettinger, W.J., Warren, J.A., Beckermann, C. and Karma, A., 2002. Phase-field simulation of solidification. *Annual review of materials research*, 32(1), pp.163–194.
- [17] Huang, Z.F., Elder, K.R. and Provatas, N., 2010. Phase-field-crystal dynamics for binary systems: Derivation from dynamical density functional theory, amplitude equation formalism, and applications to alloy heterostructures. *Physical Review E*, 82(2), p.021605.
- [18] Archer, A.J., Ratliff, D.J., Rucklidge, A.M. and Subramanian, P., 2019. Deriving phase field crystal theory from dynamical density functional theory: consequences of the approximations. *Physical Review E*, 100(2), p.022140.
- [19] Rietkerk, Max and Van de Koppel, Johan. Regular pattern formation in real ecosystems. *Trends in ecology & evolution*, 23(3):169–175, 2008.
- [20] Fabio Borgono, Paolo D’Oro, Francesco Laio, and Luca Ridolfi. *Mathematical models of vegetation pattern formation in ecohydrology*, 2009.
- [21] G. Hardin. Competitive Exclusion Principle. *Science* 131, 1292, 1960.
- [22] Robert MacArthur and Richard Levins. The limiting similarity, convergence, and divergence of coexisting species. *The American Naturalist*, 101(921):377–385, 1967.
- [23] Simone Pigolotti, Cristóbal López, and Emilio Hernández-García. Species clustering in competitive lotka-volterra models. *Physical review letters*, 98(25):258101, 2007.
- [24] Scheffer, Marten and van Nes, Egbert H. Self-organized similarity, the evolutionary emergence of groups of similar species. *Proceedings of the National Academy of Sciences*, 103(16):6230–6235, 2006.
- [25] Kuehn, Christian and Throm, Sebastian. Validity of amplitude equations for nonlocal nonlinearities. *Journal of Mathematical Physics*, 59(7):071510, 2018.
- [26] Morgan, David and Dawes, Jonathan HP. The Swift–Hohenberg equation with a nonlocal nonlinearity. *Physica D: Nonlinear Phenomena*, 270:60–80, 2014.
- [27] Fort, H., Scheffer, M. and van Nes, E.H., 2009. The paradox of the clumps mathematically explained. *Theoretical Ecology*, 2(3), pp.171–176.
- [28] Pigolotti, S., Lopez, C., Hernandez-Garcia, E. and Andersen, K.H., 2010. How Gaussian competition leads to lumpy or uniform species distributions. *Theoretical Ecology*, 3(2), pp.89–96.
- [29] Ronald Aylmer Fisher. The Wave of Advance of Advantageous Genes. *Annals of Eugenics*, 7: 355–369, 1937.
- [30] Garlaschi, S., Gupta, D., Maritan, A., and Azaele, S. See supplementary material.
- [31] Jacopo Grilli, György Barabás, Matthew J Michalska-Smith, and Stefano Allesina. Higher-order interactions stabilize dynamics in competitive network models. *Nature*, 548(7666):210–213, 2017.

# Supplemental Material for “Universal Amplitude Equation at the Onset of Pattern Formation for General Non-local and Non-linear Models”

## DERIVATION OF THE AMPLITUDE EQUATION (9)

In this section, we provide detailed calculation to obtain the evolution equation (*amplitude equation*) for amplitude of the patterns. Let us begin with a generic non-linear non-local equation describing the temporal evolution for a real field  $\phi(x, t)$ :

$$\partial_t \phi(x, t) = F_{\mathbf{q}}[\phi(x, t), (G_{\mathbf{q}} * \phi)(x, t)] + D \partial_x^2 \phi(x, t), \quad (\text{S1})$$

where  $F_{\mathbf{q}}(\cdot, \cdot)$  is a generic analytical non-linear function in its variables,  $D$  a diffusive constant, and  $(G_{\mathbf{p}} * \phi)$  the convolution between the field and an even function  $G_{\mathbf{p}}(z)$ :

$$(G_{\mathbf{q}} * \phi)(x, t) = \int_{-\infty}^{+\infty} G_{\mathbf{q}}(|x - y|) \phi(y, t) dy. \quad (\text{S2})$$

Notice that the above equation indicates the non-local contribution to the evolution of the field in Eq. (S1). In what follows, we define  $\mathbf{p} = \{\mathbf{q}, D\}$  as a set of all parameters of the system described by Eq. (S1).

### Sufficient condition for pattern formation

The patterns originate from the unstable nature of the homogeneous and stationary solution  $\phi_{\mathbf{q}}^{(0)}$ , which is the solution of

$$F_{\mathbf{q}}\left(\phi_{\mathbf{q}}^{(0)}, \tilde{G}_{\mathbf{q}}(0) \phi_{\mathbf{q}}^{(0)}\right) = 0, \quad (\text{S3})$$

where  $\tilde{G}_{\mathbf{q}}(k) = \int_{-\infty}^{+\infty} G_{\mathbf{q}}(z) e^{ikz} dz$  is the Fourier transform of the function  $G_{\mathbf{q}}(z)$ .

The stability of the homogeneous stationary solution can be understood by employing the linear stability analysis in which we add a harmonic perturbation to  $\phi_{\mathbf{q}}^{(0)}$ , i.e.,  $\phi_k(x, t) = \phi_{\mathbf{q}}^{(0)} + \delta e^{\lambda t + ikx} + c.c.$ , where  $0 < \delta \ll 1$ , and we study how such perturbation evolves in time using Eq. (S1). If the amplitude of perturbation grows in time, the homogeneous solution is unstable; otherwise, it is stable. Up to first order in  $\delta$  (i.e., in the linear regime), the dispersion relation for the growth rate  $\lambda$  as a function of  $k$  reads

$$\lambda_{\mathbf{p}}(k) = \left(1, \tilde{G}_{\mathbf{q}}(k)\right) \cdot \nabla F_{\mathbf{q}}\big|_{(\phi_{\mathbf{q}}^{(0)}, \tilde{G}_{\mathbf{q}}(0) \phi_{\mathbf{q}}^{(0)})} - Dk^2, \quad (\text{S4})$$

where  $\lambda_{\mathbf{p}}(k)$  is an even function and admits real values due to the symmetric nature of the function  $G_{\mathbf{q}}(\cdot)$ .

As discussed above, the stability of  $\phi_{\mathbf{q}}^{(0)}$  depends on the sign of  $\lambda_{\mathbf{p}}(k)$ , i.e., the homogeneous stationary solution is stable if  $\lambda_{\mathbf{p}}(k) < 0$  for all  $k$ ; otherwise,  $\phi_{\mathbf{q}}^{(0)}$  is an unstable solution. In fact, the stability of  $\phi_{\mathbf{q}}^{(0)}$  depends on the system parameters  $\mathbf{p}$ . Therefore, we can find regions in the parameter space to indicate the stability of the solution. Let us call  $k_M(\mathbf{p})$ , a solution of  $\partial_k \lambda_{\mathbf{p}}(k)|_{k=k_M(\mathbf{p})} = 0$ , a point where the growth rate achieves maximum i.e.,  $\lambda_M(\mathbf{p}) = \lambda_{\mathbf{p}}(k_M(\mathbf{p}))$ . Notice that both  $\lambda_{\mathbf{p}}(k)$  and  $k_M(\mathbf{p})$  are parameterized by system parameters  $\mathbf{p}$ . Thus, a sufficient condition that the parameters have to fulfill in order to observe pattern formation is  $\lambda_M(\mathbf{p}) > 0$ . Therefore, in the parameter space a *critical hypersurface*  $\mathcal{M}$  can be obtained by setting  $\lambda_M \equiv \lambda_{\mathbf{p}_0}(k_M(\mathbf{p}_0)) = 0$  where  $\mathbf{p}_0$  belongs to  $\mathcal{M}$ , and this hypersurface distinguishes the regions depending on the stability of  $\phi_{\mathbf{q}}^{(0)}$ .

### Amplitude equation

The instability of  $\phi_{\mathbf{q}}^{(0)}$  with respect to initial perturbations results in the formation of patterns. Consequently, temporal evolution of the perturbation could lead us in understanding the evolution of patterns. To study this

behavior, we write  $\phi(x, t) = \phi_{0, \mathbf{q}} + \varphi(x, t)$ , where  $|\varphi(x, t)| \ll |\phi_{0, \mathbf{q}}|$ , and insert it in Eq. (S1). Now we expand the right-hand side of (S1) about  $(\phi_{\mathbf{q}}^{(0)}, \tilde{G}(0)\phi_{\mathbf{q}}^{(0)})$ , and get

$$\dot{\varphi} = \mathcal{L}_{\mathbf{p}}\varphi + \mathcal{N}_{\mathbf{q}}\varphi, \quad (\text{S5})$$

where the first and second term, respectively, on the right-hand side correspond to linear and non-linear contributions in  $\varphi$ . In the above equation (S5), the linear operator has the following structure

$$\mathcal{L}_{\mathbf{p}}\varphi = (\varphi, G_{\mathbf{q}} * \varphi) \cdot \nabla F_{\mathbf{q}}|_{(\phi_{\mathbf{q}}^{(0)}, \tilde{G}_{\mathbf{q}}(0)\phi_{\mathbf{q}}^{(0)})} + D\partial_x^2\varphi = C_{\mathbf{q}}^{(1,0)}\varphi + C_{\mathbf{q}}^{(0,1)}(G_{\mathbf{q}} * \varphi) + D\partial_x^2\varphi, \quad (\text{S6})$$

while the non-linear operator is

$$\mathcal{N}_{\mathbf{q}}\varphi = \sum_{\substack{n, m=0 \\ \text{with } n+m \geq 2}}^{+\infty} C_{\mathbf{q}}^{(n,m)}\varphi^n (G_{\mathbf{q}} * \varphi)^m, \quad (\text{S7})$$

where  $C_{\mathbf{q}}^{(n,m)}$  are the coefficients obtained from the Taylor expansion.

The eigenfunctions of the linear operator are in the form  $e^{ikx}$  and its spectrum is defined by Eq. (S4), i.e.,  $\mathcal{L}_{\mathbf{p}}e^{ikx} = \lambda_{\mathbf{p}}(k)e^{ikx}$ , where

$$\lambda_{\mathbf{p}}(k) = C_{\mathbf{q}}^{(1,0)} + C_{\mathbf{q}}^{(0,1)}\tilde{G}_{\mathbf{q}}(k) - Dk^2. \quad (\text{S8})$$

Now to understand the evolution of the patterns, we consider a set of parameters  $\mathbf{p}$  in the pattern forming region (Fig. 1 of main text) in the close vicinity of the critical hypersurface  $\mathcal{M}$  such as

$$\mathbf{p} = \mathbf{p}_0 + \epsilon^2\hat{v}, \quad (\text{S9})$$

where  $\hat{v}$  is a unit vector that describes the direction of the point  $\mathbf{p}$  from  $\mathbf{p}_0$ , and  $0 < \epsilon^2 \ll 1$  measures the distance from the bifurcation.

Since we are close to the bifurcation, we expand the growth rate around  $\mathbf{p}_0$  as

$$\lambda_{\mathbf{p}}(k) = \lambda_{\mathbf{p}_0}(k) + \epsilon^2\hat{v} \cdot \nabla_{\mathbf{p}}\lambda_{\mathbf{p}}(k)|_{\mathbf{p}=\mathbf{p}_0} + O(\epsilon^4). \quad (\text{S10})$$

We know that the above function achieves a maximum at  $k = k_M(\mathbf{p})$ , and that  $k_M(\mathbf{p})$  can also be expanded about  $\mathbf{p}_0$

$$k_M(\mathbf{p}) = k_M(\mathbf{p}_0) + \epsilon^2\hat{v} \cdot \nabla_{\mathbf{p}}k_M|_{\mathbf{p}=\mathbf{p}_0} + O(\epsilon^4) \quad (\text{S11})$$

Substituting Eq. (S11) in Eq. (S10) at  $k = k_M(\mathbf{p})$ , we get

$$\begin{aligned} \lambda_M &\equiv \lambda_{\mathbf{p}}(k_M(\mathbf{p})) = \lambda_{\mathbf{p}_0}(k_M(\mathbf{p})) + \epsilon^2\hat{v} \cdot \nabla_{\mathbf{p}}\lambda_{\mathbf{p}}(k_M(\mathbf{p}))|_{\mathbf{p}=\mathbf{p}_0} + O(\epsilon^4) \\ &= \underbrace{\lambda_{\mathbf{p}_0}(k_M(\mathbf{p}_0))}_{=0} + \epsilon^2\hat{v} \cdot \nabla_{\mathbf{p}}k_M|_{\mathbf{p}=\mathbf{p}_0} \underbrace{\lambda'_{\mathbf{p}_0}(k_M(\mathbf{p}_0))}_{=0} + \underbrace{\epsilon^2\hat{v} \cdot \nabla_{\mathbf{p}}\lambda_{\mathbf{p}}(k_M(\mathbf{p}_0))|_{\mathbf{p}=\mathbf{p}_0}}_{\bar{\lambda}_M} + O(\epsilon^4) \end{aligned} \quad (\text{S12})$$

Therefore, we can clearly see that  $\lambda_M$  scales like  $\epsilon^2$  when  $\epsilon \rightarrow 0^+$ , i.e.,

$$\lambda_M \rightarrow \epsilon^2\bar{\lambda}_M \quad \text{as} \quad \epsilon \rightarrow 0^+, \quad (\text{S13})$$

where  $\bar{\lambda}_M \sim \mathcal{O}(1)$ .

This scaling relation suggests that close to the bifurcation, the pattern evolves on a longer time scale defined by a new slow variable  $\tau = \epsilon^2 t$ . Similarly, we assume the spatial evolution of the patterns described by slow spatial variable  $\xi = \epsilon x$ , where  $x$  is the fast spatial variable. Thus, the perturbing field  $\varphi$  depends on time through the new variable  $\tau$ , while the spatial dependence is through both  $x$  and  $\xi$ , i.e.,  $\varphi(x, \xi, \tau)$ . Due to these separation of scales, the time derivative transforms as

$$\partial_t \rightarrow \epsilon^2 \partial_\tau, \quad (\text{S14})$$

while the spatial derivative encoded in the linear operator becomes

$$\partial_x \rightarrow \partial_x + \epsilon \partial_\xi. \quad (\text{S15})$$

Now, we write  $\varphi(x, \xi, \tau)$  as a perturbative expansion:

$$\varphi(x, \xi, \tau) = \sum_{i \geq 1} \epsilon^i \varphi_i(x, \xi, \tau), \quad (\text{S16})$$

where  $\epsilon$  is the small parameter as introduced in Eq. (S9), and  $\varphi_i$  a real function indicating the contribution to the perturbing field at each order in  $\epsilon$ . From the above expression (S16), we see that close to the bifurcation, only first terms will be dominant and that will determine the growth of the patterns.

Similar to Eqs. (S10) and (S11), we also expand the linear and non-linear operators appearing in Eq. (S5):

$$\mathcal{L}_{\mathbf{p}} = \mathcal{L}_{\mathbf{p}_0} + \epsilon^2 \overbrace{\hat{v} \cdot (\nabla_{\mathbf{p}} \mathcal{L}_{\mathbf{p}})}^{\delta \mathcal{L}_{\mathbf{p}_0}} \Big|_{\mathbf{p}=\mathbf{p}_0} + O(\epsilon^4) \quad (\text{S17})$$

$$\mathcal{N}_{\mathbf{q}} = \mathcal{N}_{\mathbf{q}_0} + \epsilon^2 \hat{v} \cdot (\vec{\nabla}_{\mathbf{p}} \mathcal{N}_{\mathbf{q}}) \Big|_{\mathbf{p}=\mathbf{p}_0} + O(\epsilon^4) \quad (\text{S18})$$

Finally, substituting Eqs. (S14)–(S18) into Eq. (S5) gives

$$\begin{aligned} \epsilon^3 \dot{\varphi}_1 + O(\epsilon^3) &= \epsilon (\mathcal{L}_{\mathbf{p}_0} \varphi_1) + \epsilon^2 \left( \mathcal{L}_{\mathbf{p}_0} \varphi_2 + C_{\mathbf{q}_0}^{(2,0)} \varphi_1^2 + C_{\mathbf{q}_0}^{(1,1)} \varphi_1 (G_{\mathbf{q}_0} * \varphi_1) + C_{\mathbf{q}_0}^{(0,2)} (G_{\mathbf{q}_0} * \varphi_1)^2 \right) + \\ &+ \epsilon^3 \left( \mathcal{L}_{\mathbf{p}_0} \varphi_3 + \delta \mathcal{L}_{\mathbf{p}_0} \varphi_1 + 2C_{\mathbf{q}_0}^{(2,0)} \varphi_1 \varphi_2 + C_{\mathbf{q}_0}^{(1,1)} [\varphi_1 (G_{\mathbf{q}_0} * \varphi_2) + \varphi_2 (G_{\mathbf{q}_0} * \varphi_1)] + \right. \\ &+ 2C_{\mathbf{q}_0}^{(0,2)} (G_{\mathbf{q}_0} * \varphi_1) (G_{\mathbf{q}_0} * \varphi_2) + C_{\mathbf{q}_0}^{(3,0)} \varphi_1^3 + C_{\mathbf{q}_0}^{(2,1)} \varphi_1^2 (G_{\mathbf{q}_0} * \varphi_1) + \\ &\left. + C_{\mathbf{q}_0}^{(1,2)} \varphi_1 (G_{\mathbf{q}_0} * \varphi_1)^2 + C_{\mathbf{q}_0}^{(0,3)} (G_{\mathbf{q}_0} * \varphi_1)^3 \right). \end{aligned} \quad (\text{S19})$$

In the above Eq. (S19), we have only introduced the temporal-scale separation. However, we have to also incorporate the spatial scale separation in that equation (for example, the linear operator  $\mathcal{L}_{\mathbf{p}_0}$  is still a function of the spatial variable  $x$ , not of both  $x$  and  $\xi$ ). Using Eq. (S15), we can see that

$$\partial_x^2 \rightarrow (\partial_x + \epsilon \partial_\xi)^2 = \partial_x^2 + 2\epsilon \partial_x \partial_\xi + \epsilon^2 \partial_\xi^2, \quad (\text{S20})$$

and that would be helpful for the transformation of the Laplacian operator in the  $\mathcal{L}_{\mathbf{p}_0}$  from variable  $x$  to both  $x$  and  $\xi$ . Similarly, the convolutions between the function  $G_{\mathbf{q}_0}(x)$  and  $\varphi_i(x, \xi, \tau)$  in Eq. (S19) becomes

$$(G_{\mathbf{q}_0} * \varphi_i)(x, \xi, \tau) = \int_{-\infty}^{+\infty} G_{\mathbf{q}_0}(x-y) \varphi_i(y, \xi', \tau) dy, \quad (\text{S21})$$

where  $\xi = \epsilon x$  and  $\xi' = \epsilon y$ , have to be properly evaluated in order to account all possible contributions. Following [S26], we write the above integration (S21) as

$$(G_{\mathbf{q}_0} * \varphi_i)(x, \xi, \tau) = \int_{-\infty}^{+\infty} G_{\mathbf{q}_0}(-z) \varphi_i(x+z, \xi + \epsilon z, \tau) dz. \quad (\text{S22})$$

Expanding the above equation about the slow variable  $\xi$ , and integrating term by term, yields

$$(G_{\mathbf{q}_0} * \varphi_i)(x, \xi, \tau) = \sum_{n=0}^{\infty} \frac{\epsilon^n}{n!} (G_{\mathbf{q}_0} * \varphi_i)_n, \quad (\text{S23})$$

where we define

$$(G_{\mathbf{q}_0} * \varphi_i)_n(x, \xi, \tau) = \int_{-\infty}^{+\infty} G_{\mathbf{q}_0}(-z) z^n \frac{\partial^n \varphi_i}{\partial \xi^n}(x+z, \xi, \tau) dz. \quad (\text{S24})$$

Using Eqs. (S20) and (S23), the linear operator can be written as

$$\mathcal{L}_{\mathbf{p}_0} = \sum_{n=0}^{\infty} \epsilon^n \mathcal{L}_{\mathbf{p}_0}^{(n)}, \quad (\text{S25})$$



in which

$$\begin{aligned}
\mathcal{L}_{\mathbf{p}_0}^{(0)}\varphi_i(x, \xi, \tau) &= C_{\mathbf{q}_0}^{(1,0)}\varphi_i(x, \xi, \tau) + C_{\mathbf{q}_0}^{(0,1)}(G_{\mathbf{q}_0} * \varphi_i)_0(x, \xi, \tau) + D_0\partial_x^2\varphi_i(x, \xi, \tau), \\
\mathcal{L}_{\mathbf{p}_0}^{(1)}\varphi_i(x, \xi, \tau) &= C_{\mathbf{q}_0}^{(0,1)}(G_{\mathbf{q}_0} * \varphi_i)_1(x, \xi, \tau) + 2D_0\partial_x\partial_\xi\varphi_i(x, \xi, \tau), \\
\mathcal{L}_{\mathbf{p}_0}^{(2)}\varphi_i(x, \xi, \tau) &= \frac{1}{2}C_{\mathbf{q}_0}^{(0,1)}(G_{\mathbf{q}_0} * \varphi_i)_2(x, \xi, \tau) + D_0\partial_\xi^2\varphi_i(x, \xi, \tau), \\
\mathcal{L}_{\mathbf{p}_0}^{(n \geq 3)}\varphi_i(x, \xi, \tau) &= \frac{1}{n!}C_{\mathbf{q}_0}^{(0,1)}(G_{\mathbf{q}_0} * \varphi_i)_n(x, \xi, \tau).
\end{aligned}$$

Finally, Eq. (S19) becomes

$$\begin{aligned}
\epsilon^3\dot{\varphi}_1 + o(\epsilon^3) &= \epsilon \left( \mathcal{L}_{\mathbf{p}_0}^{(0)}\varphi_1 \right) + \epsilon^2 \left( \mathcal{L}_{\mathbf{p}_0}^{(0)}\varphi_2 + C_{\mathbf{q}_0}^{(2,0)}\varphi_1^2 + C_{\mathbf{q}_0}^{(1,1)}\varphi_1(G_{\mathbf{q}_0} * \varphi_1)_0 + C_{\mathbf{q}_0}^{(0,2)}(G_{\mathbf{q}_0} * \varphi_1)_0^2 + \mathcal{L}_{\mathbf{p}_0}^{(1)}\varphi_1 \right) + \\
&+ \epsilon^3 \left( \mathcal{L}_{\mathbf{p}_0}^{(0)}\varphi_3 + \delta\mathcal{L}_{\mathbf{p}_0}^{(0)}\varphi_1 + 2C_{\mathbf{q}_0}^{(2,0)}\varphi_1\varphi_2 + C_{\mathbf{q}_0}^{(1,1)}[\varphi_1(G_{\mathbf{q}_0} * \varphi_2)_0 + \varphi_2(G_{\mathbf{q}_0} * \varphi_1)_0] + \right. \\
&+ 2C_{\mathbf{q}_0}^{(0,2)}(G_{\mathbf{q}_0} * \varphi_1)_0(G_{\mathbf{q}_0} * \varphi_2)_0 + C_{\mathbf{q}_0}^{(3,0)}\varphi_1^3 + C_{\mathbf{q}_0}^{(2,1)}\varphi_1^2(G_{\mathbf{q}_0} * \varphi_1)_0 C_{\mathbf{q}_0}^{(1,2)} + \varphi_1(G_{\mathbf{q}_0} * \varphi_1)_0^2 + \\
&\left. + C_{\mathbf{q}_0}^{(0,3)}(G_{\mathbf{q}_0} * \varphi_1)_0^3 + \mathcal{L}_{\mathbf{p}_0}^{(2)}\varphi_1 + \mathcal{L}_{\mathbf{p}_0}^{(1)}\varphi_2 + C_{\mathbf{q}_0}^{(1,1)}\varphi_1(G_{\mathbf{q}_0} * \varphi_1)_1 + 2C_{\mathbf{q}_0}^{(0,2)}(G_{\mathbf{q}_0} * \varphi_1)_0(G_{\mathbf{q}_0} * \varphi_1)_1 \right). \tag{S26}
\end{aligned}$$

In the following, we compare the terms on the LHS and RHS of Eq. (S26) of the same order of  $\epsilon$  to compute the different contributions of the perturbative expansion.

#### $O(\epsilon)$ contribution

At the lowest order in  $\epsilon$ , we find from Eq. (S26) that

$$\mathcal{L}_{\mathbf{p}_0}^{(0)}\varphi_1 = 0, \tag{S27}$$

and therefore, it is straightforward to write the solution of this equation as

$$\varphi_1(x, \xi, \tau) = A(\xi, \tau)e^{ik_M(\mathbf{p}_0)x} + \bar{A}(\xi, \tau)e^{-ik_M(\mathbf{p}_0)x}. \tag{S28}$$

The functional form of  $\varphi_1(x, \xi, \tau)$  suggests that it has harmonic oscillation with the mode characterized by  $k_M(\mathbf{p}_0)$ . We further notice that, the temporal dependence is only present through the amplitude of this harmonic oscillation on a slower scale defined by  $\tau$ . Moreover, such amplitude may display a spatial evolution, but on the longer scale given by  $\xi$ . Near the criticality, we expect that it is the relevant contribution to the pattern formation. Thus, to understand the growth of the patterns near bifurcation, we aim to obtain the equation for that amplitude.

#### $O(\epsilon^2)$ contribution

On grouping the second order terms in Eq. (S26), we obtain

$$\mathcal{L}_{\mathbf{p}_0}^{(0)}\varphi_2 = -C_{\mathbf{q}_0}^{(2,0)}\varphi_1^2 - C_{\mathbf{q}_0}^{(1,1)}\varphi_1(G_{\mathbf{q}_0} * \varphi_1)_0 - C_{\mathbf{q}_0}^{(0,2)}(G_{\mathbf{q}_0} * \varphi_1)_0^2 - \mathcal{L}_{\mathbf{p}_0}^{(1)}\varphi_1. \tag{S29}$$

In order to find the solution  $\varphi_2$  we need to evaluate  $(G_{\mathbf{q}_0} * \varphi_1)_0$  and  $\mathcal{L}_{\mathbf{p}_0}^{(1)}\varphi_1$ . Using Eqs. (S24) and (S28), we get

$$(G_{\mathbf{q}_0} * \varphi_1)_0(x, \xi, \tau) = \int_{-\infty}^{+\infty} G_{\mathbf{q}_0}(-z) \left[ A(\epsilon x, \tau)e^{ik_M(\mathbf{p}_0)(x+z)} + \bar{A}(\epsilon x, \tau)e^{-ik_M(\mathbf{p}_0)(x+z)} \right] dz. \tag{S30}$$

Thanks to the even nature of the function  $G_{\mathbf{q}_0}(z)$ , we find

$$\begin{aligned}
(G_{\mathbf{q}_0} * \varphi_1)_0(x, \xi, \tau) &= \tilde{G}_{\mathbf{q}_0}(k_M(\mathbf{p}_0)) \left[ A(\xi, \tau)e^{ik_M(\mathbf{p}_0)x} + \bar{A}(\xi, \tau)e^{-ik_M(\mathbf{p}_0)x} \right] \\
&= \tilde{G}_{\mathbf{q}_0}(k_M(\mathbf{p}_0))\varphi_1(x, \xi, \tau).
\end{aligned} \tag{S31}$$

Let us now evaluate  $\mathcal{L}_{\mathbf{p}_0}^{(1)}\varphi_1$  and we get

$$\mathcal{L}_{\mathbf{p}_0}^{(1)}\varphi_1 = C_{\mathbf{q}_0}^{(0,1)}(G_{\mathbf{q}_0} * \varphi_1)_1 + 2D_0\partial_x\partial_\xi\varphi_1, \quad (\text{S32})$$

where

$$(G_{\mathbf{q}_0} * \varphi_1)_1(x, \xi, \tau) = (\partial_\xi A)(\epsilon x, \tau)e^{ik_M(\mathbf{p}_0)x}I + (\partial_\xi \bar{A})(\epsilon x, \tau)e^{-ik_M(\mathbf{p}_0)x}\bar{I} \quad (\text{S33})$$

in which the integral

$$I = \int_{-\infty}^{+\infty} G_{\mathbf{q}_0}(-z)ze^{ik_M(\mathbf{p}_0)z}dz = -i\tilde{G}'(k_M(\mathbf{p}_0)), \quad (\text{S34})$$

and  $\bar{I}$  is its complex conjugate. Therefore,  $\mathcal{L}_{\mathbf{p}_0}^{(1)}\varphi_1$  becomes

$$\mathcal{L}_{\mathbf{p}_0}^{(1)}\varphi_1 = i\partial_\xi A(\xi, \tau)e^{ik_M(\mathbf{p}_0)x} \underbrace{\lambda'_{\mathbf{p}_0}(k_M(\mathbf{p}_0))}_{=0} + i\partial_\xi \bar{A}(\xi, \tau)e^{-ik_M(\mathbf{p}_0)x} \underbrace{\lambda'_{\mathbf{p}_0}(-k_M(\mathbf{p}_0))}_{=0} = 0. \quad (\text{S35})$$

Using Eqs. (S31), (S33), and (S35) in Eq. (S29), we finally get

$$\mathcal{L}_{\mathbf{p}_0}^{(0)}\varphi_2 = \Sigma_{\mathbf{p}_0}\varphi_2^2, \quad (\text{S36})$$

where we define the coefficient  $\Sigma_{\mathbf{p}_0}$  as

$$\Sigma_{\mathbf{p}_0} = -C_{\mathbf{q}_0}^{(2,0)} - C_{\mathbf{q}_0}^{(1,1)}\tilde{G}_{\mathbf{q}_0}(k_M(\mathbf{p}_0)) - C_{\mathbf{q}_0}^{(0,2)}\tilde{G}_{\mathbf{q}_0}(k_M(\mathbf{p}_0))^2$$

Clearly, Eq. (S36) satisfies the Fredholm's alternative since  $\varphi_1^2 \notin \ker(\mathcal{L}_{\mathbf{p}_0}^{(0)})$ . In fact, the right-hand side of Eq. (S36) is orthogonal to  $\varphi_1$ , and therefore, using Fredholm's alternative, Eq. (S29) admits a bounded solution.

Using Eq. (S28) in (S36), we obtain the solution  $\varphi_2(x, \xi, \tau)$  of Eq. (S36)

$$\varphi_2(x, \xi, \tau) = \Sigma_{\mathbf{p}_0} \left( \frac{A^2(\xi, \tau)e^{2ik_M(\mathbf{p}_0)x}}{\lambda_{\mathbf{p}_0}(2k_M(\mathbf{p}_0))} + 2\frac{|A|^2(\xi, \tau)}{\lambda_{\mathbf{p}_0}(0)} + \frac{\bar{A}^2(\xi, \tau)e^{-2ik_M(\mathbf{p}_0)x}}{\lambda_{\mathbf{p}_0}(2k_M(\mathbf{p}_0))} \right) + \overbrace{B(\xi, \tau)e^{ik_M(\mathbf{p}_0)x} + \bar{B}(\xi, \tau)e^{-ik_M(\mathbf{p}_0)x}}^{\Lambda(x, \xi, \tau)}, \quad (\text{S37})$$

where the first term on the right-hand side and  $\Lambda(x, \xi, \tau)$ , respectively, are the particular and homogeneous solutions Eq. (S36).

### $O(\epsilon^3)$ contribution and the G-L amplitude equation

In the following, we compare the terms of third order in  $\epsilon$  in the expansion (S26). Therefore, we get

$$\begin{aligned} -\mathcal{L}_{\mathbf{p}_0}^{(0)}\varphi_3 &= -\dot{\varphi}_1 + \delta\mathcal{L}_{\mathbf{p}_0}^{(0)}\varphi_1 + 2C_{\mathbf{q}_0}^{(2,0)}\varphi_1\varphi_2 + C_{\mathbf{q}_0}^{(1,1)}[\varphi_1(G_{\mathbf{q}_0} * \varphi_2)_0 + \varphi_2(G_{\mathbf{q}_0} * \varphi_1)_0] + \\ &+ 2C_{\mathbf{q}_0}^{(0,2)}(G_{\mathbf{q}_0} * \varphi_1)_0(G_{\mathbf{q}_0} * \varphi_2)_0 + C_{\mathbf{q}_0}^{(3,0)}\varphi_1^3 + C_{\mathbf{q}_0}^{(2,1)}\varphi_1^2(G_{\mathbf{q}_0} * \varphi_1)_0C_{\mathbf{q}_0}^{(1,2)} + \varphi_1(G_{\mathbf{q}_0} * \varphi_1)_0^2 + \\ &+ C_{\mathbf{q}_0}^{(0,3)}(G_{\mathbf{q}_0} * \varphi_1)_0^3 + \mathcal{L}_{\mathbf{p}_0}^{(2)}\varphi_1 + \mathcal{L}_{\mathbf{p}_0}^{(1)}\varphi_2 + C_{\mathbf{q}_0}^{(1,1)}\varphi_1(G_{\mathbf{q}_0} * \varphi_1)_1 + 2C_{\mathbf{q}_0}^{(0,2)}(G_{\mathbf{q}_0} * \varphi_1)_0(G_{\mathbf{q}_0} * \varphi_1)_1. \end{aligned} \quad (\text{S38})$$

We substitute the expression of  $(G_{\mathbf{q}_0} * \varphi_2)_0$  [following Eqs. (S24) and (S37)],  $\delta\mathcal{L}_{\mathbf{p}_0}^{(0)}\varphi_1$ , and  $\mathcal{L}_{\mathbf{p}_0}^{(2)}\varphi_1$ :

$$\begin{aligned} (G_{\mathbf{q}_0} * \varphi_2)_0(x, \xi, \tau) &= \Sigma_{\mathbf{p}_0} \left\{ \frac{\tilde{G}_{\mathbf{q}_0}(2k_M(\mathbf{p}_0))}{\lambda_{\mathbf{p}_0}(2k_M(\mathbf{p}_0))} \left[ A^2(\xi, \tau)e^{2ik_M(\mathbf{p}_0)x} + \bar{A}^2(\xi, \tau)e^{-2ik_M(\mathbf{p}_0)x} \right] + \frac{2\tilde{G}_{\mathbf{q}_0}(0)}{\lambda_{\mathbf{p}_0}(0)} |A(\xi, \tau)|^2 \right\} + \\ &+ \tilde{G}_{\mathbf{q}_0}(k_M(\mathbf{p}_0))\Lambda(x, \xi, \tau), \end{aligned} \quad (\text{S39})$$

$$\delta\mathcal{L}_{\mathbf{p}_0}\varphi_1 = \hat{v} \cdot \left( \vec{\nabla}_{\mathbf{p}} \mathcal{L}_{\mathbf{p}} \right) \Big|_{\mathbf{p}=\mathbf{p}_0} \varphi_1 \equiv \bar{\lambda}_M \varphi_1, \quad (\text{S40})$$

$$\mathcal{L}_{\mathbf{p}_0}^{(2)}\varphi_1 = \frac{1}{2}C_{\mathbf{q}_0}^{(0,1)}(G_{\mathbf{q}_0} * \varphi_1)_2 + D_0\partial_\xi^2\varphi_1, \quad (\text{S41})$$

in Eq. (S38), where

$$(G_{\mathbf{q}} * \varphi_1)_2(x, \xi, \tau) = -\tilde{G}''(k_M(\mathbf{p}_0))\partial_\xi^2 A(\xi, \tau)e^{ik_M(\mathbf{p}_0)x} - \tilde{G}''(-k_M(\mathbf{p}_0))\partial_\xi^2 \bar{A}(\xi, \tau)e^{-ik_M(\mathbf{p}_0)x}. \quad (\text{S42})$$

Notice that in arriving the above form of  $(G_{\mathbf{q}} * \varphi_1)_2(x, \xi, \tau)$  we have used the same strategy as in Eq. (S33). Thus, Eq. (S41) becomes

$$\mathcal{L}_{\mathbf{p}_0}^{(2)}\varphi_1 = -\frac{1}{2}\lambda_{\mathbf{p}_0}''(k_M(\mathbf{p}_0))\partial_\xi^2 A(\xi, \tau)e^{ik_M(\mathbf{p}_0)x} - \frac{1}{2}\lambda_{\mathbf{p}_0}''(-k_M(\mathbf{p}_0))\partial_\xi^2 \bar{A}(\xi, \tau)e^{-ik_M(\mathbf{p}_0)x}. \quad (\text{S43})$$

Finally, we substitute Eqs. (S39), (S40), (S43), and  $\varphi_1$  from Eq. (S28) in Eq. (S38). Since  $\varphi_3$  has to be bounded, the RHS of Eq. (S38) must be orthogonal to  $\varphi_1$  (Fredholm's alternative). Therefore, setting the coefficients of  $e^{ik_M(\mathbf{p}_0)x}$  in Eq. (S38) equal to zero while noticing that  $\mathcal{L}_{\mathbf{p}_0}^{(1)}\varphi_2 + C_{\mathbf{q}_0}^{(1,1)}\varphi_1(G_{\mathbf{q}_0} * \varphi_1)_1 + 2C_{\mathbf{q}_0}^{(0,2)}(G_{\mathbf{q}_0} * \varphi_1)_0 (G_{\mathbf{q}_0} * \varphi_1)_1$  does not have any term proportional to  $e^{ik_M(\mathbf{p}_0)x}$ , we obtain the GL amplitude equation:

$$\frac{\partial A}{\partial \tau} = \bar{\lambda}_M A - \alpha |A|^2 A + \frac{1}{2} |\lambda_{\mathbf{p}_0}''(k_M(\mathbf{p}_0))| \frac{\partial^2 A}{\partial \xi^2}, \quad (\text{S44})$$

where  $\bar{\lambda}_M$  is given in (S12) and the coefficient  $\alpha$  has the following form:

$$\begin{aligned} \alpha = & -\left\{ 2\Sigma_{\mathbf{p}_0} C_{\mathbf{q}_0}^{(2,0)} \left[ \frac{2}{\lambda_{\mathbf{p}_0}(0)} + \frac{1}{\lambda_{\mathbf{p}_0}(2k_M(\mathbf{p}_0))} \right] + \Sigma_{\mathbf{p}_0} C_{\mathbf{q}_0}^{(1,1)} \left[ 2 \frac{\tilde{G}_{\mathbf{q}_0}(0) + \tilde{G}_{\mathbf{q}_0}(k_M(\mathbf{p}_0))}{\lambda_{\mathbf{p}_0}(0)} + \right. \right. \\ & \left. \left. + \frac{\tilde{G}_{\mathbf{q}_0}(0) + \tilde{G}_{\mathbf{q}_0}(2k_M(\mathbf{p}_0))}{\lambda_{\mathbf{p}_0}(2k_M(\mathbf{p}_0))} \right] + 2\Sigma_{\mathbf{p}_0} C_{\mathbf{q}_0}^{(0,2)} \tilde{G}_{\mathbf{q}_0}(k_M(\mathbf{p}_0)) \left[ \frac{2\tilde{G}_{\mathbf{q}_0}(0)}{\lambda_{\mathbf{p}_0}(0)} + \frac{\tilde{G}_{\mathbf{q}_0}(2k_M(\mathbf{p}_0))}{\lambda_{\mathbf{p}_0}(2k_M(\mathbf{p}_0))} \right] + \right. \\ & \left. + 3C_{\mathbf{q}_0}^{(3,0)} + 3C_{\mathbf{q}_0}^{(2,1)} \tilde{G}_{\mathbf{q}_0}(k_M(\mathbf{p}_0)) + 3C_{\mathbf{q}_0}^{(1,2)} (\tilde{G}_{\mathbf{q}_0}(k_M(\mathbf{p}_0)))^2 + 3C_{\mathbf{q}_0}^{(0,3)} (\tilde{G}_{\mathbf{q}_0}(k_M(\mathbf{p}_0)))^3 \right\}. \quad (\text{S45}) \end{aligned}$$

## PARTICULAR SOLUTIONS OF THE GL AMPLITUDE EQUATION

In this section, we present two interesting analytical solutions of the GL amplitude equation (S44).

Let us substitute the complex amplitude  $A(\xi, \tau)$ :

$$A(\xi, \tau) = |A(\xi, \tau)|e^{i\theta(\xi, \tau)} \quad (\text{S46})$$

where both  $|A(\xi, \tau)|$  and  $\theta(\xi, \tau)$  are real functions of  $\xi$  and  $\tau$ , in Eq. (S44). Separating the real and imaginary parts, we obtain a set of coupled differential equations for the modulus  $|A(\xi, \tau)|$  and the phase of the amplitude  $\theta(\xi, \tau)$ :

$$\partial_\tau |A| = \bar{\lambda}_M |A| - \alpha |A|^3 + \frac{1}{2} |\lambda_{\mathbf{p}_0}''(k_M(\mathbf{p}_0))| [\partial_\xi^2 |A| - |A|(\partial_\xi \theta)^2], \quad (\text{S47})$$

$$|A| \partial_\tau \theta = \frac{1}{2} |\lambda_{\mathbf{p}_0}''(k_M(\mathbf{p}_0))| [2(\partial_\xi |A|)(\partial_\xi \theta) + |A| \partial_\xi^2 \theta], \quad (\text{S48})$$

where, for convenience, we have dropped the arguments in both  $|A(\xi, \tau)|$  and  $\theta(\xi, \tau)$ .

It is difficult to obtain the solution of above coupled differential for a generic initial condition. Nonetheless, for some particular initial conditions, the exact solution can be obtained. As a first example, we consider an initial homogeneous condition, i.e.,

$$A(\xi, 0) \equiv A_0 e^{i\theta_0}, \quad (\text{S49})$$

where both  $A_0$  and  $\theta_0$  are independent of  $\xi$ . Therefore, the solution in this case can be obtained as

$$|A(\xi, \tau)| = \frac{A_0 \sqrt{\bar{\lambda}_M} \exp(\bar{\lambda}_M \tau)}{\sqrt{\bar{\lambda}_M + A_0^2 \alpha [\exp(2\bar{\lambda}_M \tau) - 1]}}, \quad (\text{S50})$$

$$\theta(\xi, \tau) = \theta_0, \quad (\text{S51})$$

and they satisfy both Eq. (S47) and (S48) and the initial condition Eq. (S49). Thus, for a given initial homogeneous condition, the GL amplitude equation predicts the amplitude to be homogeneous where only the modulus  $|A|$  evolves with time  $\tau$ .

To obtain a spatial solution of the amplitude equation, we again consider an initial homogeneous condition for the phase, i.e.,  $\theta(\xi, 0) \equiv \theta_0$ . Thus, the equation for the modulus of the amplitude reduces to

$$\partial_\tau |A| = \bar{\lambda}_M |A| - \alpha |A|^3 + \frac{1}{2} |\lambda''_{\mathbf{p}_0}(k_M(\mathbf{p}_0))| \partial_\xi^2 |A| \quad (\text{S52})$$

A steady solution  $|A_{st}(\xi)|$  of above Eq. (S52) can be obtained by setting the left hand side of Eq. (S52) to 0, and we get

$$|A_{st}(\xi)| = \pm \sqrt{\frac{\bar{\lambda}_M}{\alpha}} \tanh \left[ \xi \sqrt{\frac{\bar{\lambda}_M}{|\lambda''(k_M(\mathbf{p}_0))|}} \right]. \quad (\text{S53})$$

as one possible solution, as shown in Ref. [2] of the main text.

Since  $|A_{st}(\xi)|$  must be non-negative, a solution that satisfies this condition can be constructed as

$$|A_{st}(\xi)| = \sqrt{\frac{\bar{\lambda}_M}{\alpha}} \tanh \left[ |\xi| \sqrt{\frac{\bar{\lambda}_M}{|\lambda''(k_M(\mathbf{p}_0))|}} \right]. \quad (\text{S54})$$

In the above solution, we consider both solutions (S53) depending on the sign of the variable  $\xi$  and introduce a defect at  $\xi = 0$ , where the amplitude becomes zero. In fact, this solution also satisfies the amplitude equation everywhere except at the defect where it changes the behavior passing from one to the other solution displayed in Eq. (S53).

It is possible to show analytically that the homogeneous solution of Eq. (S44) is linearly stable while the steady spatial one (S53) is locally linearly unstable. In other words, the numerical spatial solution is a good approximation of the analytical prediction only up to a finite observation time. Indeed, because of numerical inaccuracies, at larger time scales the profile will inevitably fall into the basin of attraction of the stationary stable solution.

In the following section, we compare the theoretical prediction of the amplitude with the numerical simulation of discrete CLV model.

## NUMERICAL METHODS

In this section, we discuss the method of numerical simulation to verify the analytical prediction of the amplitude equation (9) of the main text. As an example, we consider the discrete Competitive Lotka-Volterra (CLV) model of  $N$  species where each one is located equidistant from the nearest-neighbor species on a one-dimensional ring where the spatial variable  $x$  ranges from  $-L$  to  $L$ . Thus, the  $i$ -th species is present at

$$x_i = -L + i dx \quad \text{where } i = 1, \dots, N, \quad (\text{S55})$$

with  $x_N = x_0$  [i.e., periodic boundary condition (PBC)]. In the above equation,  $dx = 2L/N$  is the uniform spacing.

The population of these species evolve according the following dynamics

$$\partial_t \phi_i(t) = \phi_i(t) \left[ 1 - a \sum_{j=1}^N G_{\mathbf{q}}(\min\{|i-j|dx, 2L-|i-j|dx\}) \phi_j(t) \right] + D \Delta \phi_i(t). \quad (\text{S56})$$

where the interaction kernel respects PBC. The above equations (S56) are supplemented with initial conditions  $\phi_i(t=0)$  which we will discuss later.

In the above Eq. (S56), the subscript  $i$  corresponds to  $i$ -th species and the discrete Laplacian operator  $\Delta$  acting on the field  $\phi_i$  is defined as

$$\Delta \phi_i = \frac{\phi_{i-1} - 2\phi_i + \phi_{i+1}}{dx^2}.$$

The homogeneous and stationary solution corresponding to Eq. (S56) is given by

$$\begin{aligned} \phi_{\mathbf{q}}^{(0)} &= \frac{1}{a \sum_{j=1}^N G_{\mathbf{q}}(\min\{|i-j|dx, 2L-|i-j|dx\})} \\ &= \frac{1}{2a \sum_{j=1}^{\frac{N}{2}-1} G_{\mathbf{q}}(j dx) + a G_{\mathbf{q}}(L) + a G_{\mathbf{q}}(0)}. \end{aligned} \quad (\text{S57})$$

Now, to understand the stability of  $\phi_{\mathbf{q}}^{(0)}$ , we substitute  $\phi_j(t) \equiv \phi_{\mathbf{p}}^{(0)} + \delta e^{\lambda_{\mathbf{p}}(k_n)t + ik_n x_j} + c.c.$ , where  $0 < \delta \ll 1$  and  $k_n = n\frac{\pi}{L}$  with  $n$  being an integer, in Eq. (S56). Therefore, we obtain the following dispersion relation (up to a linear order in  $\delta$ )

$$\lambda_{\mathbf{p}}(k_n) = -\frac{\tilde{g}_{\mathbf{q}}(k_n)}{\tilde{g}_{\mathbf{q}}(0)} + 2D \frac{\cos(k_n dx) - 1}{dx^2}, \quad (\text{S58})$$

where we have introduced the discrete Fourier transform as

$$\tilde{g}_{\mathbf{q}}(k_n) = 2 \sum_{j=1}^{\frac{N}{2}-1} \cos(k_n j dx) G_{\mathbf{q}}(j dx) + (-1)^n G_{\mathbf{q}}(L) + G_{\mathbf{q}}(0). \quad (\text{S59})$$

In the following, we describe the recipe to obtain the amplitude of the pattern formed near the critical hypersurface  $\mathcal{M}$  (Fig. 1 of the main text) by numerical simulating Eq. (S56). We stress that the theoretical prediction of amplitude equation [see Eq. (9) of the main text] does not get affected for the above discussed model. In this case, we just replace the Fourier transform [defined in Eq. (S3)] with its discrete counterpart (S59).

First, we consider a point  $\mathbf{p}$  in the pattern forming region (See Fig. 1 of the main text) and find the value of  $\lambda_M$  using Eq. (S58), where  $\lambda_M = \max_{k_n} \{\lambda_{\mathbf{p}}(k_n)\}$ . Then we take the point  $\mathbf{p}_0$ , that lies on  $\mathcal{M}$  around which we perform the expansion as discussed in the main text, and we compute  $k_M(\mathbf{p}_0)$  and the coefficients appearing in Eq. (9) of the main text.

We note that in general for the continuous model shown in Eq. 1 of the main text, the analytical solution of the dynamics [using solution of Eq. (9) of the main text given initial conditions, and Eq. (S16)] can be written as (up to first order in  $\epsilon$ )

$$\begin{aligned} \phi(x, \xi, \tau) &\approx \phi_{\mathbf{q}}^{(0)} + \epsilon \varphi_1(x, \xi, \tau) \\ &\approx \phi_{\mathbf{q}}^{(0)} + 2\epsilon |A(\xi, \tau)| \cos[k_M(\mathbf{p}_0)x + \theta(\xi, \tau)], \end{aligned} \quad (\text{S60})$$

where  $A(\xi, \tau) = |A(\xi, \tau)|e^{i\theta(\xi, \tau)}$ . Therefore, the analogous discrete version of the above solution is

$$\phi_i(\xi_i, \tau) = \phi(x_i, \xi_i, \tau) \approx \phi_{\mathbf{q}}^{(0)} + 2\epsilon |A(\xi_i, \tau)| \cos[k_M(\mathbf{p}_0)x_i + \theta(\xi_i, \tau)], \quad (\text{S61})$$

where  $x_i$  corresponds to discrete spatial location of the  $i$ -th species.

Here we aim to compare the amplitude given in the Eq. (S61) with the numerical simulation. To do so, we use the same initial and boundary conditions imposed on the solution (S61). Finally, we verify the analytical prediction for growth of the amplitude for two different initial conditions given in Eqs. (S50), (S51), and (S54) in Figs. S1 and S2.

### SCALING RELATION FOR $\lambda_M$ AND WIDTH $\mathcal{K}$

In this section, we present the numerical result for the scaling relation between the maximum  $\lambda_M$  (defined in the main text) and  $\mathcal{K}$ , where  $\mathcal{K} = k_+ - k_-$ , where  $k_{\pm}$  are the solution of equation  $\lambda(k) = 0$ , for the CLV model. In Fig. S3, we plot the maximum of  $\lambda(k)$  with respect to  $\mathcal{K}$  as we change  $b$  for fixed parameters  $\beta = 0.2$ ,  $D = 10^{-8}$ , and  $R = 0.1$  (solid curve), and compare with the quadratic prediction (dashed curve). It is clear from the figure that near the bifurcation point, the height of  $\lambda(k)$  grows quadratically with the width  $\mathcal{K}$ .

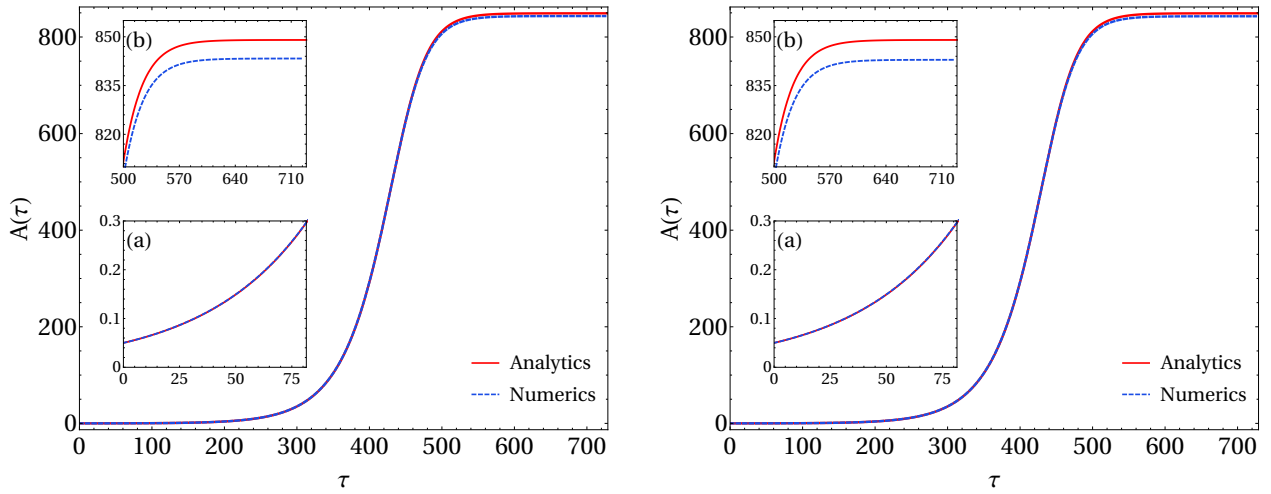


FIG. S1. Comparison between theoretical prediction of the GL amplitude equation (S44) with the initial condition  $A(\xi_i, 0) = |A(\xi_i, 0)| = A_0 = 0.05$  (solid red line) and the amplitude obtained from the numerical simulation (blue dashed line) for the discrete CLV model where the system is initialized in the state  $\phi_i(\xi_i, 0) = \phi(x_i, \xi_i, 0) = \phi_{\mathbf{q}}^{(0)} + 2\epsilon A_0 \cos[k_M(\mathbf{p}_0)x_i]$ . In the numerical implementation, we take  $N = 3060$  species equispaced along a ring of length  $2L = 3$ , and these are interacting among each others with an interaction kernel given by  $G_{\mathbf{q}}(z) = \exp\left(-\frac{|z|}{R}\right) - b \exp\left(-\frac{|z|}{\beta R}\right)$ . In the left panel, the amplitude is extracted from the numerical simulation exploiting Eq. (S61) whereas in the right panel, we employ the truncated series (S16) up to second order to estimate the amplitude from the same numerical simulation. Insets in the two plots show the zooming of the curves up to a particular range of time  $\tau$ . Both plots are shown for fixed sets of parameters  $\mathbf{p}$  and  $\mathbf{p}_0$ . In particular, here we set  $R = 0.1$ ,  $\beta = 0.5851$ ,  $b = 0.6$ ,  $a = 10^{-4}$ , and  $D = 10^{-8}$ . To compute the coefficients of Eq. (S44) we used the set  $\mathbf{p}_0$  in which we tuned  $\beta$  leaving the other parameters fixed.

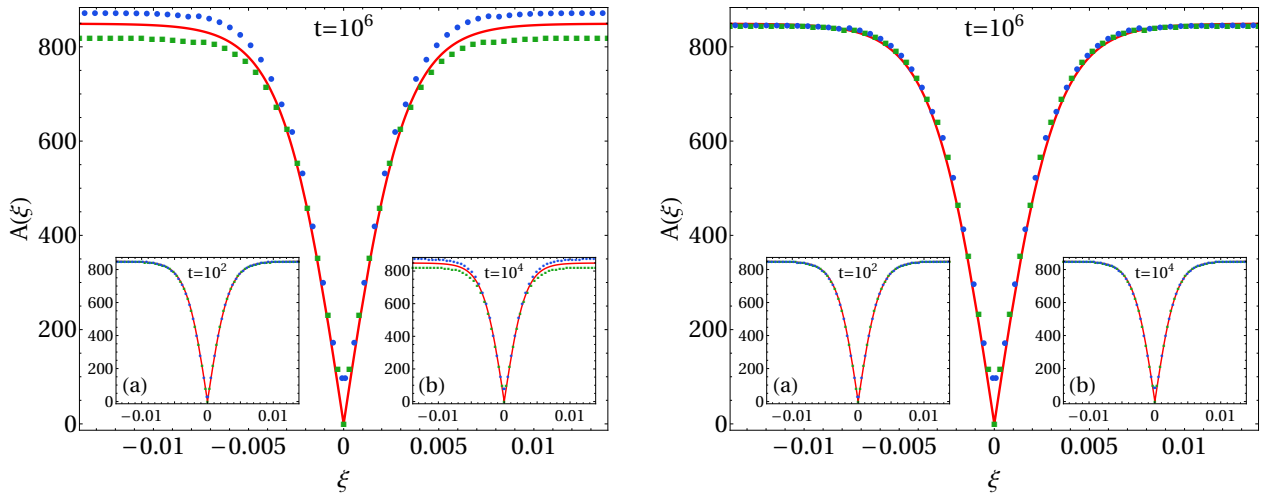


FIG. S2. Comparison of theoretical prediction of the GL amplitude equation (S44) (solid red line) with the numerical simulation (blue circles and green squares) for the discrete CLV model using the defective steady solution  $A_{st}(\xi)$  (S54) and  $\phi_i(\xi_i, 0) = \phi(x_i, \xi_i, 0) = \phi_{\mathbf{q}}^{(0)} + 2\epsilon A_{st}(\xi_i) \cos[k_M \mathbf{p}_0 x_i]$ , respectively, as initial conditions. From the numerical integration of the discrete CLV dynamics, we extract the envelope of the pattern using its local maxima (circles) and minima (squares). In the left panel, the amplitude is extracted from the numerical simulation exploiting Eq. (S61) whereas in the right panel, we use the truncated series (S16) up to second order to estimate the amplitude from the same numerical simulation. We show in the main plots the comparison at  $t = 10^6$  of the discrete CLV dynamics, while in the insets the comparison is displayed at  $t = 10^2$  (a) and  $t = 10^4$  (b). Clearly, we can see that when we consider the higher-order contribution the agreement improves at larger time. The simulated dynamics, including the interaction kernel and the sets of parameter  $\mathbf{p}$  and  $\mathbf{p}_0$  used, is the same one presented in the caption of Figure S1, where the initial condition has been changed.

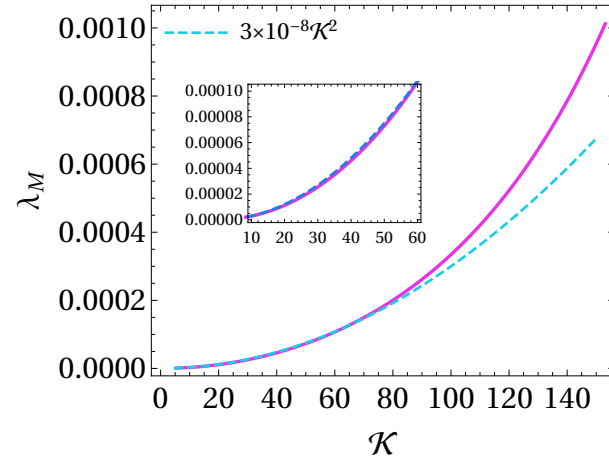


FIG. S3. Scaling relation between  $\lambda_M$  and  $\mathcal{K}$  as a function of  $b$ . The plot is shown for fixed parameters  $\beta = 0.2$ ,  $D = 10^{-8}$ , and  $R = 0.1$ .